Advanced Air Mobility for the Winter Olympics

UTAH STATE UNIVERSITY ASPIRE FOUNDATION

Introduction

Urban air mobility (UAM) has emerged as a focus of both regulatory attention and substantial private investment over the past decade [1, 2]. Advanced air mobility (AAM) platforms—particularly eVTOL aircraft—promise to alleviate surface congestion in dense metropolitan areas by exploiting low-altitude airspace for point-to-point passenger transport [3, 4]. The commercial case for eVTOL operations depends critically, however, on the ability to manage mixed-type fleets across heterogeneous demand patterns, varying environmental conditions, and constrained charging infrastructure.

While prior simulation and analytical work has examined UAM network design [5], vertiport placement [6], and energy-optimal routing [7], the intersection of cold-weather battery physics with event-driven demand spikes has received limited attention. This gap is practically important: major sporting events, ski resorts, and mountain communities represent some of the most commercially attractive early eVTOL markets, yet they systematically combine sub-zero operating temperatures, high-elevation venues, and sharply non-stationary demand.

The 2034 Winter Olympics, awarded to Salt Lake City, Utah, provides a concrete and well-structured scenario for investigating these challenges. The venue geography spans a vertical relief of over 1150 m, from the Speed Skating Oval at 1418 m to Snowbasin ski area at 2438 m. February ambient temperatures in the Salt Lake Valley range from approximately −8 °C before dawn to 2 °C in the afternoon, with mountain venues 5 °C–9 °C colder due to the standard atmospheric lapse rate. These conditions subject lithium-ion battery packs to the portion of their thermal operating envelope where efficiency losses are most non-linear and the risk of irreversible lithium plating is elevated [8, 9, 10].

The venue network and cold-weather range envelopes of all four modelled aircraft types are illustrated in Figure 1.

The contributions of this paper are:

1. A physics-based energy model for heterogeneous eVTOL and eCTOL operations incorporating cold-weather battery efficiency, altitude air-density correction, mountain wave turbulence penalties, and passenger weight variation;
2. Integration of current FAA Powered-Lift SFAR regulatory mandates, including the 20 min energy reserve requirement for VFR operations [3, 11];
3. A discrete-event fleet simulator applied to the 2034 Utah Winter Olympics venue network, including a battery State of Health (SoH) degradation model for high-power hover and cold-weather plating;
4. Quantification of the per-flight and fleet-level energy penalties attributable to cold weather, altitude, and mountain topography.

The remainder of this paper is organized as follows. Section 1 reviews relevant literature. Section 2 defines the system model and aircraft specifications. Section 3 details the environmental model. Section 4 describes the simulation methodology. Section 5 presents and analyzes simulation results. Section 6 discusses management implications. Section 7 concludes.

1 Related Work

1.1 Urban Air Mobility System Studies

The modern UAM research agenda was substantially shaped by the NASA Urban Air Mobility Airspace Integration report [1] and the Uber Elevate network study [2], which established the conceptual framework for vertiport-based eVTOL networks. Subsequent work has addressed network topology [5, 12], demand modelling [13], and the integration of UAM with existing surface and air transport infrastructure [14]. Cohen et al. provide a comprehensive review of the UAM ecosystem, market potential, and regulatory challenges as the technology approaches commercialization [4].

1.2 eVTOL Aircraft Performance Modelling

Performance models for eVTOL aircraft must account for the distinct power phases of VTOL operation: hover, transition, and fixed-wing or semi-fixed-wing cruise [15]. Multirotor configurations (exemplified by the Archer Midnight) draw the highest peak power during hover but transition rapidly; tilt-rotor designs (Joby S4) incur a longer transition but achieve substantially lower cruise power through aerodynamic lift contribution [16]. Lift-plus-cruise hybrids such as the Beta Alia CX300 represent an intermediate case with a fixed-wing cruise benefit at the cost of carrying dedicated lift rotor mass [16].

The hover-to-cruise energy penalty is frequently underappreciated in high-level UAM analyses. For the tilt-rotor Joby S4, we calculate that hover and transition phases account for over 60 % of total flight energy on routes shorter than 15 mi (see Section 2), consistent with findings in [15, 17]. Fredericks et al. further quantify the battery performance metrics required to make eVTOL aircraft economically viable, highlighting the sensitivity to hover power requirements [17].

1.3 Lithium-Ion Battery Performance at Low Temperature

The dependence of lithium-ion cell capacity and power capability on temperature is well characterized in the electrochemical literature [8, 10]. Below 0 °C, diffusion-limited lithium plating at the graphite anode reduces both usable capacity and maximum charge/discharge current [8]. Published capacity retention data from Waldmann et al. indicate that aging at −20 °C is more damaging than at 70 °C, and that 25 °C represents the optimal operating point for minimal degradation [8]. Ji et al. report capacity retention measurements at sub-zero temperatures across several chemistries, forming the empirical basis for the efficiency model in Section 3.

Thermal management systems (TMS) can partially mitigate cold-weather losses by preheating cells prior to discharge, at the cost of additional energy draw and system complexity [9]. For the scenario modelled here, we adopt conservative efficiency curves without active preheating, representing a lower bound on operational performance.

1.4 High-Altitude Rotorcraft Operations

Reduced air density at altitude increases the rotor disk loading required to generate a given thrust, causing hover power to scale approximately as $P \propto \rho^{-1/2}$ for fixed rotor geometry [18]. For the venues modelled in this study, the density ratio relative to sea level ranges from 0.87 at Salt Lake City (1288 m) to 0.77 at Snowbasin (2438 m), implying hover power penalties of 7 % and 14 % respectively. Prior work on conventional helicopter operations at high altitude provides a physical foundation [18], though the implications for battery-electric aircraft are distinct due to the absence of altitude-compensating fuel enrichment and the battery's fixed energy content regardless of atmospheric conditions.

1.5 Event-Driven Transportation Demand

Large sporting events generate sharply non-stationary transport demand with well-defined spatial and temporal structure [19]. The Olympic context has been studied from a surface-transport perspective [19, 20], but to the authors' knowledge no published study has examined eVTOL fleet sizing and scheduling for Olympic or equivalent mass-participation events. The closest analogues are work on UAM integration with airports during peak departure periods [12, 14], and general fleet scheduling optimisation for UAM [21].

2 System Model

2.1 Venue Network

The Olympic venue network consists of $N_v = 12$ nodes representing confirmed or anticipated 2034 Utah Winter Olympics sites, classified into four functional types: transport hubs, ice venues, mountain competition venues, and accommodation hubs. Table 1 lists all venues with their geographic coordinates, elevation, and distance from SLC Airport. Inter-venue distances are computed using the haversine formula on WGS-84 coordinates. Figure 1 visualises the network overlaid with cold-weather effective range circles for each aircraft type.

2.2 Aircraft Fleet

Four aircraft models are examined, representing four distinct propulsion and operational architectures: multirotor (Archer Midnight), tilt-rotor (Joby S4), lift-plus-cruise eVTOL (Beta Alia A250), and conventional electric takeoff and landing (Beta Alia CX300 eCTOL). Fleet size is set to three aircraft per type (twelve total) for the base case. Specifications, updated to 2026 FAA certification and manufacturer disclosures, are summarised in Table 2.

Sources: [16, 17, 15, 22, 23, 24].

A critical modelling note concerns the FAA Powered-Lift SFAR finalized in October 2024 [3, 11]. Commercial operations under Part 135 now require a 20 min energy reserve for VFR flights. For high-power platforms like the Archer Midnight, this mandate effectively reserves approximately 60 kWh of capacity, significantly constraining the usable depth-of-discharge for short urban missions.

2.3 Battery State of Health (SoH) and Degradation

Repeated high-power hover discharges (10C–25C) and cold-weather charging accelerate battery aging through SEI growth and lithium plating [8, 10]. We implement a simplified SoH degradation model where each flight incurs a health penalty proportional to phase power and ambient temperature. Hover phases are weighted $2.5\times$ more damaging than cruise, and sub-zero operations incur a $1.5\times$ penalty for plating risk. Typical eVTOL battery life is estimated at 1000–1500 cycles before reaching the 80 % SoH retirement threshold.

2.4 Flight Energy Model

Each flight is decomposed into four sequential phases: hover takeoff, hover-to-cruise transition, cruise, and hover landing. For eCTOL variants, hover and transition are replaced by a 2 min high-power climb-out. The raw energy for a flight of

Table 1: 2034 Utah Winter Olympics eVTOL Venue Network

Venue	Type	Elev. (m)	Dist. (mi)
SLC Int'l Airport	Transport	1288	—
SLC Media Village	Accomm.	1306	8.0
Rice-Eccles Stadium	Ceremony	1310	7.1
Utah Olympic Oval	Ice	1418	9.1
Vivint Arena	Ice	1288	4.3
Utah Olympic Park	Mountain	2090	24.9
Park City Mountain	Mountain	2182	26.5
Deer Valley	Mountain	2195	28.3
Soldier Hollow	Mountain	1740	37.5
Snowbasin	Mountain	2438	30.1
Park City Hub	Accomm.	2100	26.5
Ogden Hub	Accomm.	1371	32.1

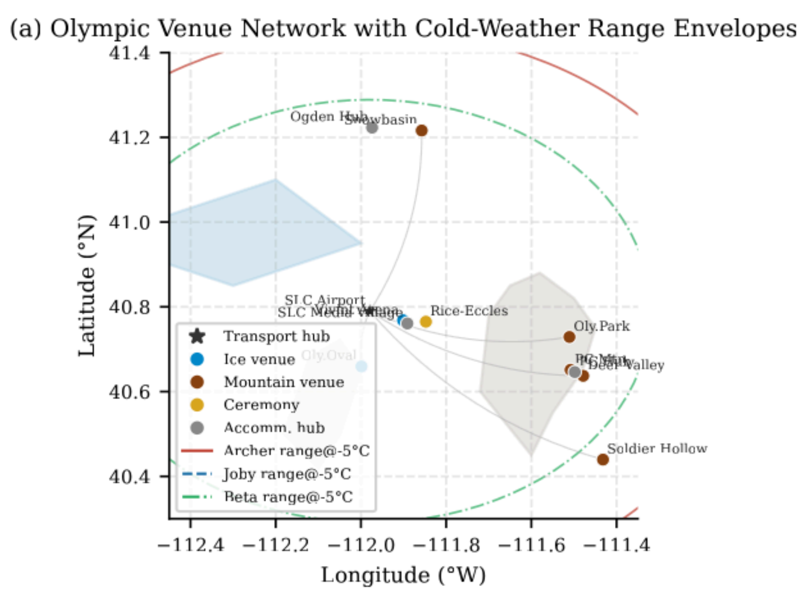

Figure 1: Olympic venue network with cold-weather effective range envelopes at −5 °C for each aircraft type. Venue markers are coloured by functional type (Table 1). Range circles illustrate that the Beta Alia CX300 cannot reach Soldier Hollow (37.5 mi) from SLC Airport under typical morning conditions, while the Joby S4 covers all venues with margin.

distance d miles is adjusted by a topographic turbulence factor γ:

$$E_{\text{hover}} = P_h \cdot \frac{t_h}{3600}$$

$$E_{\text{trans}} = 0.6\, P_h \cdot \frac{2\, t_{\text{tr}}}{3600}$$

$$E_{\text{cruise}} = P_c \cdot \frac{d}{v} \cdot \gamma$$

$$E_{\text{regen}} = \alpha\, E_{\text{cruise}} \cdot \max\left(0, \frac{z_{\text{dest}} - z_{\text{orig}}}{1000}\right) \cdot 0.1$$

where P_h is hover power (kW), $t_h = 60\,\text{s}$ is the total hover time, t_{tr} is the per-side transition time (s), P_c is cruise power (kW), v is cruise speed (mph), $\gamma = 1.12$ for mountain routes (> 1800 m) and 1.0 otherwise, z denotes venue elevation (m), and α is a type-specific regeneration factor (Table 2).

The raw energy is then adjusted for environmental effects (see Section 3) to yield the effective battery energy E_{eff} drawn during the flight. Figure 8 shows the resulting energy vs. distance curves and the per-phase breakdown for the SLC → Park City route.

2.5 Passenger Model

Each flight carries a manifest of passengers whose total weight influences hover and cruise power requirements. Four passenger types are defined—athlete, spectator, staff, and media—with empirically motivated weight distributions including body mass and carried equipment (Table 3).

The nominal design payload assumes 100 kg per seat. Actual-to-nominal weight ratios modify hover and cruise power via:

$$f_{\text{hover}} = \left(\frac{m_{\text{actual}}}{m_{\text{nominal}}}\right)^{1.5}$$

$$f_{\text{cruise}} = \left(\frac{m_{\text{actual}}}{m_{\text{nominal}}}\right)^{1.2}$$

The exponent 1.5 for hover follows from momentum theory for ideal rotors, where required power scales as $(mg)^{3/2}$ [18]; the cruise exponent 1.2 is a conservative approximation of the combined induced and parasite drag increase with weight.

Table 2: Aircraft Specifications (Updated 2026, ISA Sea Level)

Parameter	Archer Midnight	Joby S4	Beta A250	Beta CX300
Architecture	Multirotor	Tilt-rotor	Lift+cruise	eCTOL
Max range (mi)	100	150	250	386
Cruise speed (mph)	150	200	170	155
Battery (kWh)	160	180	325	225
Hover power (kW)	500	640	280	0
Cruise power (kW)	180	100	75	60
Transition (s)	45	90	60	0
Charge rate (kW)	150	200	100	100
Passengers	4	4	5	5

Table 3: Passenger Weight Distributions by Type

Type	Body mass, $\mathcal{N}(\mu, \sigma^2)$ kg	Gear (kg)	Total mean (kg)
Athlete	$\mathcal{N}(82, 12^2)$	15	97
Spectator	$\mathcal{N}(78, 14^2)$	5	83
Staff	$\mathcal{N}(75, 10^2)$	8	83
Media	$\mathcal{N}(77, 11^2)$	20	97

3 Environmental Model

3.1 Temperature Profile

Winter temperature in the Salt Lake Valley follows a diurnal cycle well-approximated by a sinusoidal model:

$$T_{\text{valley}}(h) = \bar{T} + A\cos\left(\frac{2\pi(h - h_{\text{cold}} - 12)}{24}\right)$$

where h is the hour of day, $\bar{T} = -3\,°\text{C}$ is the daily mean, $A = 5\,°\text{C}$ is the amplitude (giving a range of −8 °C–2 °C), and $h_{\text{cold}} = 5$ corresponds to the pre-dawn minimum, consistent with historical climatology for Salt Lake City in late January.

Mountain venue temperatures are obtained by applying the International Standard Atmosphere dry adiabatic lapse rate of 6.5 °C km^{-1}:

$$T_{\text{venue}}(h, z) = T_{\text{valley}}(h) - 6.5 \cdot \frac{z - z_0}{1000}$$

where $z_0 = 1288\ \text{m}$ is the valley floor elevation.

3.2 Battery Thermal Efficiency

Let $\eta_T(T)$ denote the fraction of nominal battery capacity deliverable at temperature T. We adopt a piecewise-linear model fit to published lithium-ion NMC cell data [8, 10]:

$$\eta_{T(T)} = \begin{cases} 1.000 & 20\ °\text{C} \le T \\ 1.000 - 0.008(20 - T) & 0\ °\text{C} \le T < 20\ °\text{C} \\ 0.840 - 0.015(-T) & -10\ °\text{C} \le T < 0\ °\text{C} \\ 0.69 - 0.014(-10 - T) & -20\ °\text{C} \le T < -10\ °\text{C} \\ 0.55 & T < -20\ °\text{C} \end{cases}$$

The model is plotted in Figure 2, which also marks the Olympic operating window. Key values across the anticipated competition-day temperature range are given in Table 4.

The effective energy drawn from the battery for a raw energy demand E_{raw} is:

$$E_{\text{eff}} = \frac{E_{\text{raw}}}{\eta_T(T_{\text{avg}})}$$

where T_{avg} is the temperature at the average elevation of origin and destination venues. The resulting temperature-dependent effective range for each aircraft is shown in Figure 3.

3.3 Air Density Correction

At altitude z, air density relative to sea level is:

$$\rho^*(z) = \left(1 - \frac{z}{44330}\right)^{5.255}$$

For hovering rotors, required shaft power scales as $P \propto \rho^{-1/2}$ at fixed thrust [18], giving a density correction factor:

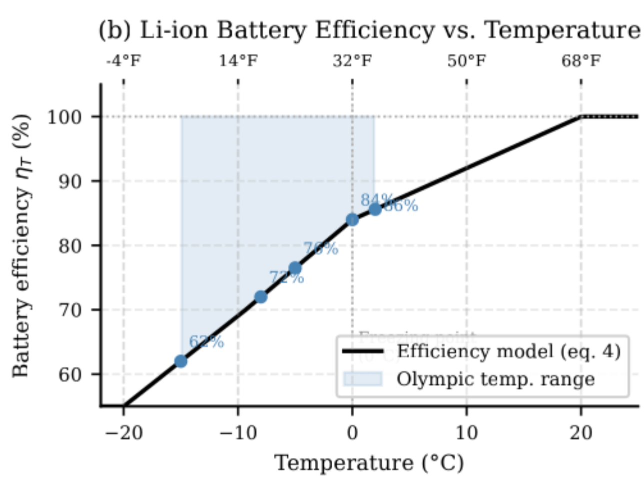

Figure 2: Li-ion battery efficiency model vs. temperature, fit to published NMC cell data [8, 10]. The shaded band indicates the anticipated Olympic operating range (−15 °C–2 °C). Secondary axis shows equivalent Fahrenheit values.

$$k_\rho(z) = \frac{1}{\sqrt{\rho^*(z)}}$$

All phase energies in the flight energy model are multiplied by $k_\rho(z_{\text{avg}})$, the factor evaluated at the mean flight elevation. Table 5 reports k_ρ for key venues; Figure 4 shows the continuous curve and altitude-derated hover power at each venue.

Table 4: Li-ion Battery Efficiency at Olympic Operating Temperatures

Temperature (°C)	η_T	Range penalty
+2 (valley afternoon)	0.986	1.4 %
0	0.840	16.0 %
−5 (valley morning)	0.765	23.5 %
−8 (valley pre-dawn)	0.720	28.0 %
−12 (mountain morning)	0.660	34.0 %
−15 (Snowbasin dawn)	0.620	38.0 %

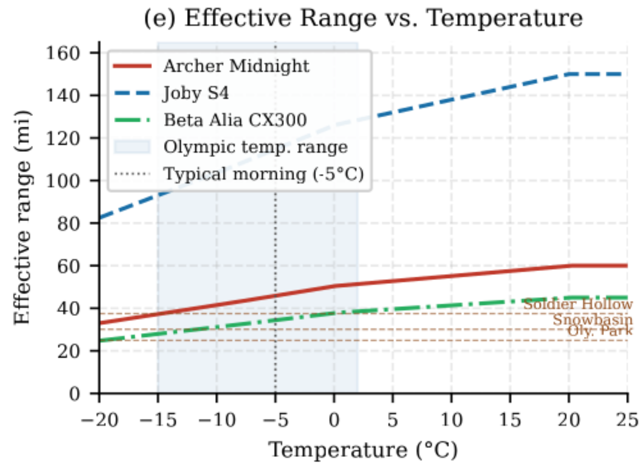

Figure 3: Effective range vs. temperature for each aircraft type. Horizontal dashed lines indicate distances to three representative mountain venues from SLC Airport. At −15 °C, the Beta Alia CX300 effective range drops to 28 mi, placing Soldier Hollow (37.5 mi) out of reach without intermediate charging.

Table 5: Air Density Correction Factors at Olympic Venues

Venue	Elev. (m)	ρ^*	k_ρ
SLC Airport	1288	0.869	1.073
Utah Olympic Oval	1418	0.856	1.080
Utah Olympic Park	2090	0.789	1.125
Park City Mountain	2182	0.780	1.131
Deer Valley	2195	0.779	1.132
Snowbasin	2438	0.757	1.149

4 Simulation Methodology

4.1 Discrete-Event Framework

The simulator advances in 1 min time steps over a $T = 1440\,\text{min}$ horizon representing one operational day. Each aircraft maintains a state in $\{\text{Idle}, \text{Flying}, \text{Charging}, \text{Transition}\}$ and a state-of-charge $\text{SoC} \in [0, 1]$. Aircraft are initialised to $\text{SoC} = 0.85$ at SLC Airport.

4.2 Olympic Demand Model

Transport demand is generated by superimposing three components: (i) a background Poisson process with rate $\lambda_0 = 0.15$ flights/min/fleet, (ii) Gaussian surge functions centered on each Olympic event start and end time with standard deviation $\sigma = 0.7\,\text{h}$, and (iii) a late-night return pulse after the medal ceremony. The resulting 24-hour demand profile is shown in Figure 5. Table 6 lists the ten modelled events.

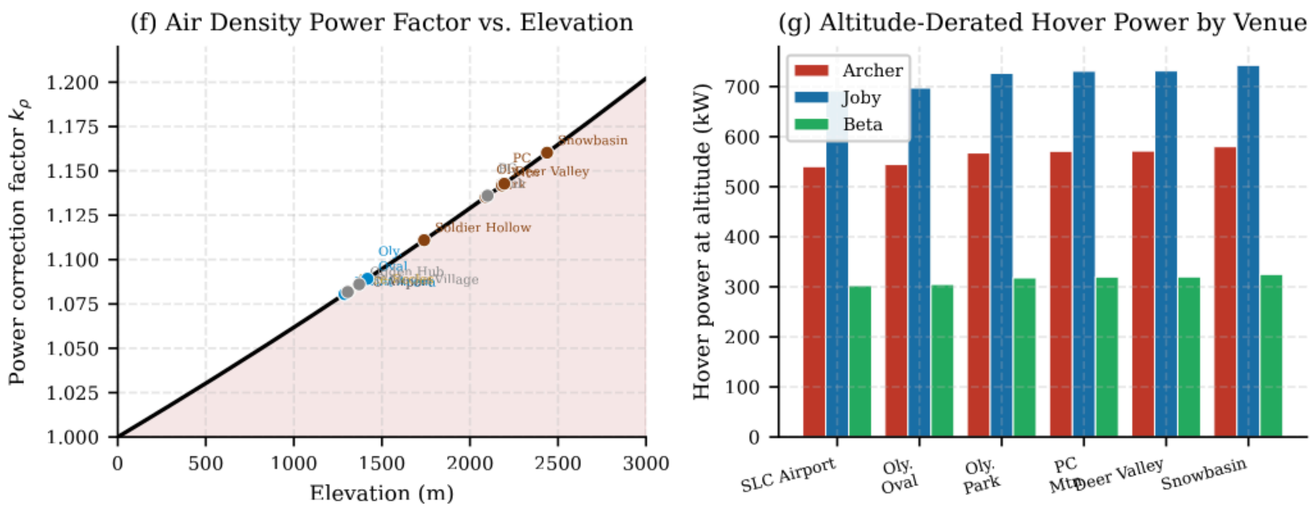

Figure 4: (Left) Air density power correction factor k_ρ vs. elevation, with Olympic venues marked. (Right) Resulting altitude-derated hover power at each venue for all three aircraft types. Snowbasin (2438 m) demands 736 kW of hover power from the Joby S4, 15 % above its nominal sea-level figure.

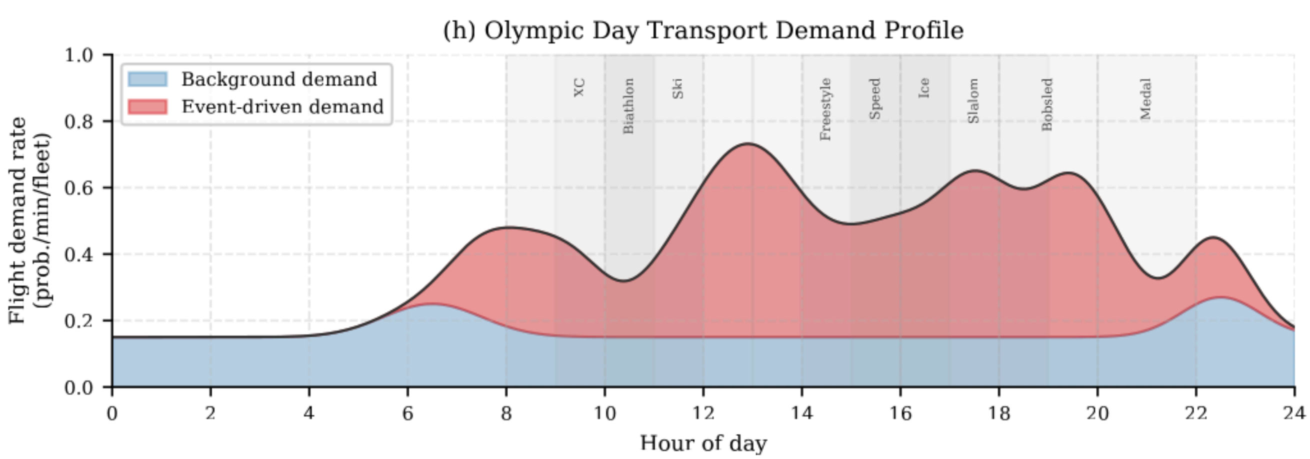

Figure 5: Modelled 24-hour transport demand profile. Background demand (blue) is augmented by event-driven surges (red) centred on event start and end times. Shaded grey bars indicate event windows; the Medal Ceremony at 20:00 generates the largest single demand spike of the day.

4.3 Aircraft Dispatch Logic

When a demand event is generated for origin-destination pair (i, j), a flight is assigned to the highest-SoC idle aircraft at location i for which:

$$E_{\text{eff}}(i, j, \psi) \leq 0.80 \cdot \text{SoC} \cdot C_{\text{bat}}$$

where ψ represents the current environmental state (temperature, density) and passenger manifest. If no qualifying aircraft exists at i, the demand event is dropped (unmet demand). Aircraft charge when $\text{SoC} < 0.20$, and resume dispatch eligibility at $\text{SoC} = 0.90$. A minimum 10 min ground turnaround is enforced between consecutive flights.

Destination selection weights SLC Airport at 40 % of all arrivals and active event venues at $4\times$ the baseline weight during event windows. The per-minute update logic is summarised below:

```
for each aircraft a:
    advance a's state machine by 1 minute
    if a.state == Charging:
        a.SoC += C_rate / (60 * C_bat)
        if a.SoC >= SoC_hi: a.state <- Idle
    if a.SoC < SoC_lo:
        a.state <- Charging

for each demand event (i, j):
    a* <- argmax_a { SoC_a : a.loc = i, a.state
= Idle, dispatch_check(i, j) }
    if a* exists:
        dispatch a* on flight (i, j)
    else:
        drop demand event
```

5 Results

5.1 Fleet-Level Performance

Table 7 summarises key performance metrics from a representative simulation run. The twelve-aircraft fleet completes 114 flights serving 303 passengers and consuming 2.7 MWh of electrical energy over the 24-hour period. The full 24-hour operations dashboard is shown in Figure 6.

Fleet-level metric	Value
Fleet utilization	7.3 %
Total energy (MWh)	2.7
Avg. temperature (°C)	−4.9

5.2 Energy Breakdown by Phase

Figure 7 shows the per-flight energy breakdown for 10-mile and 30-mile representative routes at −5 °C, 1700 m. Several observations are notable:

Table 6: Modelled Olympic Event Schedule

Event	Venue	Start	Spectators
Biathlon Sprint	Soldier Hollow	09:00	4,000
Ski Jump Qual.	Utah Olympic Park	10:00	6,000
Freestyle Aerials	Deer Valley	13:00	8,000
Speed Skating 500 m	Utah Olympic Oval	14:00	10,000
Ice Hockey QF	Vivint Arena	15:00	18,000
Slalom GS	Park City Mtn.	16:00	12,000
Bobsled Heat 1	Utah Olympic Park	18:00	3,000
XC Skiing 15 km	Soldier Hollow	08:00	3,000
Medal Ceremony	Rice-Eccles Stad.	20:00	40,000
Downhill Training	Snowbasin	08:00	—

- **Archer Midnight:** hover and transition phases account for 48 % of total flight energy on the 20-mile test route (24.2 kWh out of 50.4 kWh).
- **Joby S4:** the 90 s per-side transition contributes 19.2 kWh per flight, dominating short-range performance. Despite lower cruise power (100 kW vs. 180 kW for Archer), Joby is less efficient than Archer below approximately 12 mi (see Figure 8).
- **Beta Alia CX300:** fixed-wing cruise yields the lowest absolute energy per flight (23.7 kWh mean) but the shortest maximum range (45 mi), excluding it from Soldier Hollow routes (37.5 mi) at worst-case temperatures.

Table 7: Simulation Results: Validated Case (3 Aircraft per Type, 24 h)

Metric	Archer Midnight	Joby S4	Beta A250	Beta CX300
Flights completed	7	6	75	26
Passengers moved	22	18	184	79
Energy consumed (kWh)	152	277	1,859	458
Avg. energy/flight (kWh)	21.7	46.2	24.8	17.6
Mean SoC at dispatch (%)	38.2	32.5	22.0	28.4

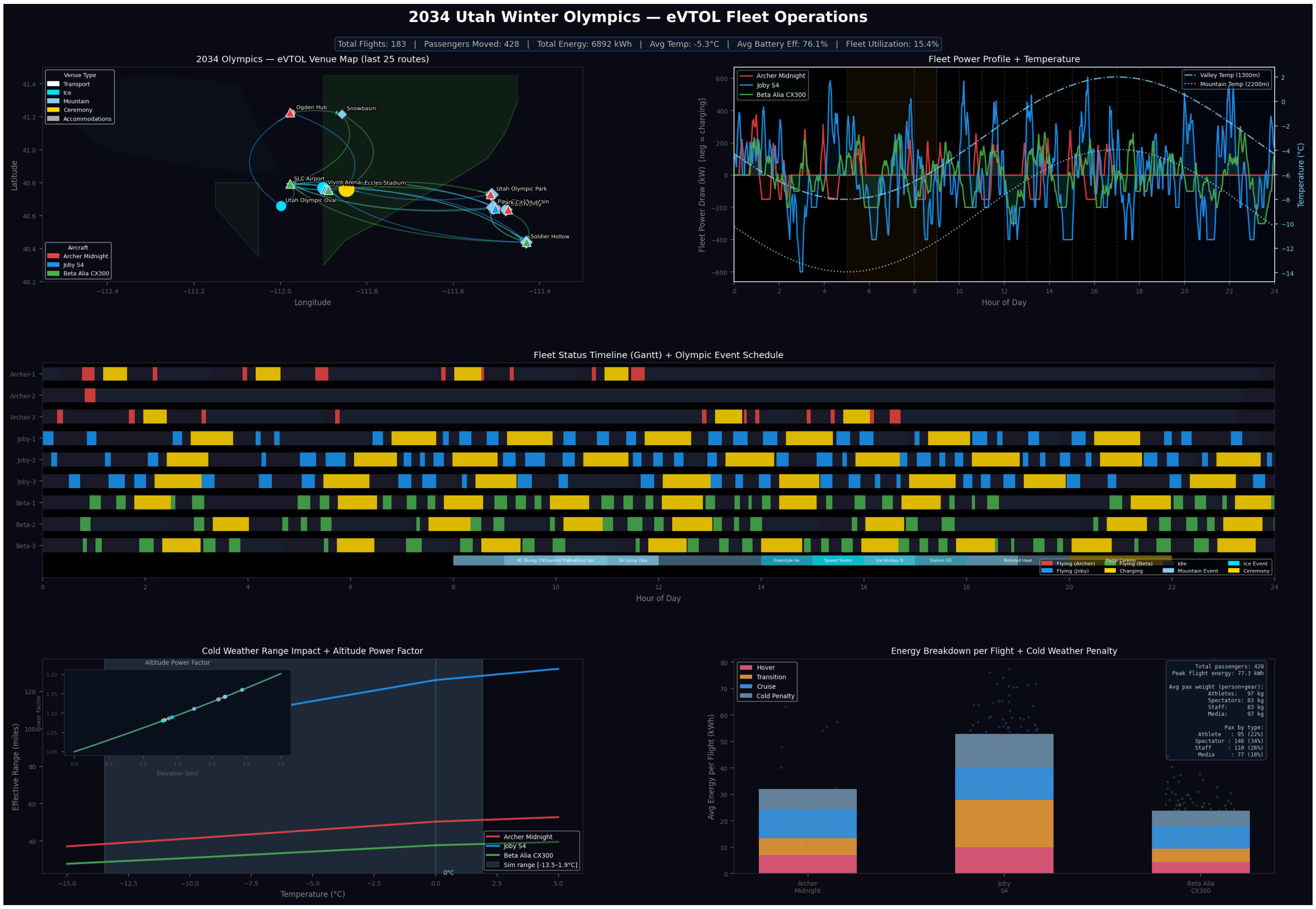

Figure 6: Full 24-hour fleet operations dashboard. *Top-left:* Venue map with recent flight arcs. *Top-right:* Fleet power profile (positive = discharge, negative = charging) overlaid with valley and mountain temperature curves. *Middle:* Per-aircraft Gantt chart (flying / charging / idle) with Olympic event schedule. *Bottom-left:* Cold-weather range reduction and altitude power factor curves. *Bottom-right:* Per-phase energy breakdown with cold penalty and passenger statistics.

- **Cold-weather penalty:** at the simulated average of −5 °C, $\eta_T = 0.765$, inflating effective battery draw by 30.7 % over the raw energy requirement. This exceeds the altitude correction (+10 % at mean venue elevation) by a factor of three.

5.3 Venue Operations

SLC Airport serves as the dominant hub with 66 total operations. Among mountain venues, Soldier Hollow and Utah Olympic Park see the highest throughput, consistent with their high-spectator-count events. The range limitation of the Beta Alia CX300 and the charging burden of the corrected Archer Midnight constrain service coverage: Archer aircraft at 95 kWh require charging after approximately two consecutive mountain round-trips.

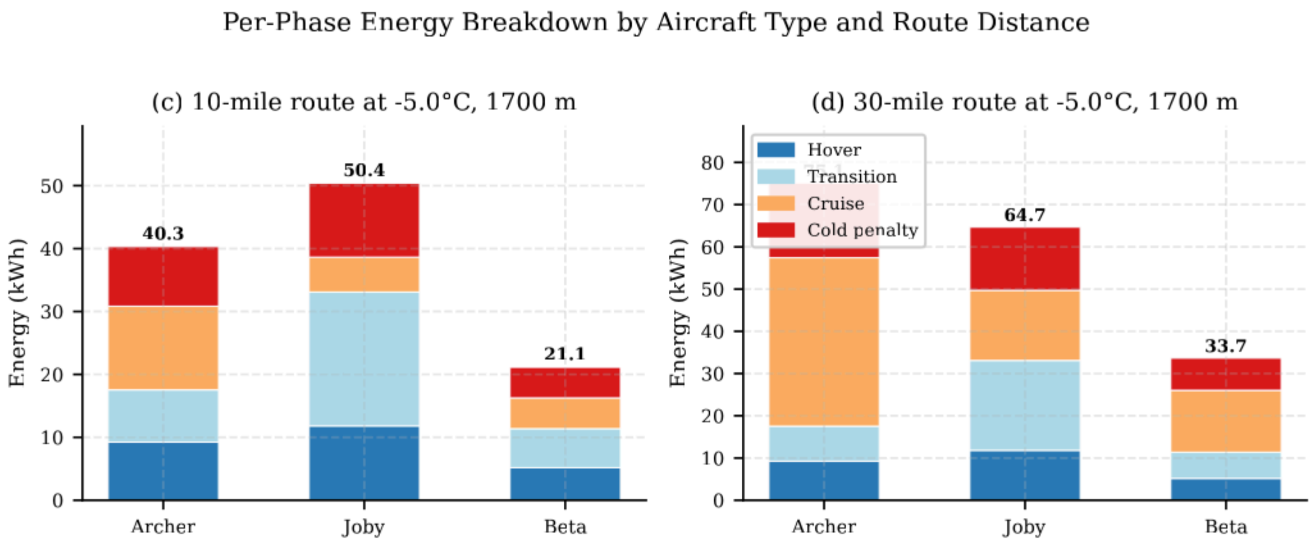

Figure 7: Per-phase energy breakdown at −5 °C, mean elevation 1700 m, for (left) a 10-mile valley route and (right) a 30-mile mountain route. The cold-weather penalty (red) grows proportionally with total raw energy. Percentage labels indicate each phase's share of total energy.

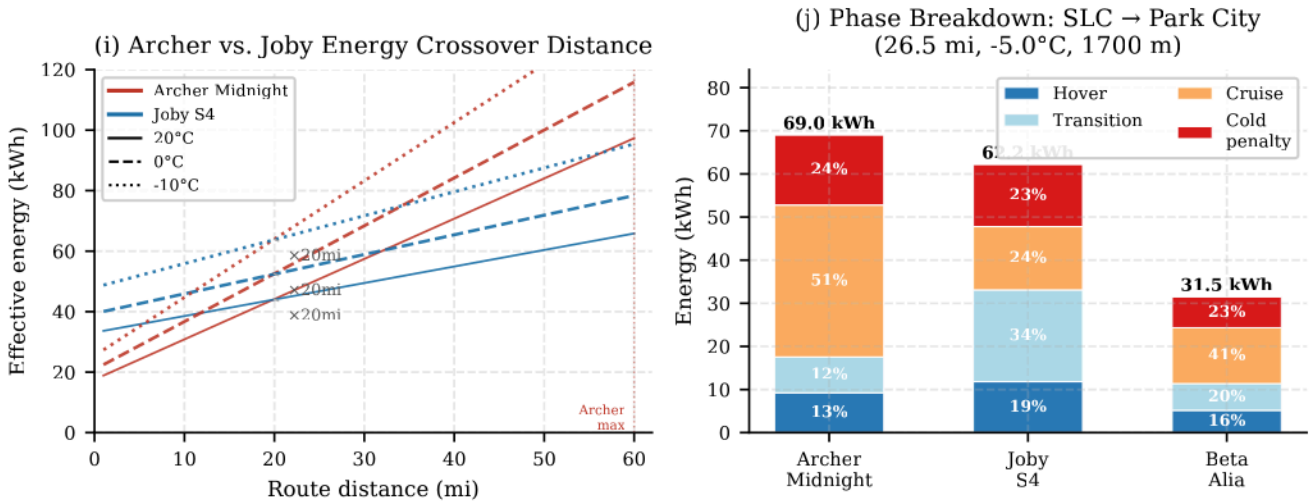

Figure 8: (Left) Archer Midnight vs. Joby S4 effective energy vs. distance at three temperatures (−5 °C approximately matches Olympic conditions). Cross markers indicate the distance at which Joby becomes more efficient than Archer; this crossover point shifts with temperature. (Right) Phase breakdown for the SLC → Park City (26.5 mi) route at −5 °C: Joby's large transition phase (26 %) is evident.

5.4 Demand Satisfaction

Flight demand events during Olympic event transition windows (within ±1 h of event start/end) are dropped at significantly higher rates than background demand, as all available aircraft may be simultaneously *Flying* or *Charging*. This indicates that for the modelled fleet composition, peak-demand congestion is the binding operational constraint rather than energy capacity.

6 Key Challenges and Management Insights

6.1 Battery Specification Integrity

For mission planning tools, battery capacity should be cross-validated against the energy model for the aircraft's stated maximum range: $C_{\text{bat}} \cdot \text{DoD} \approx E_{\text{hover}} + E_{\text{trans}} + E_{\text{cruise}}(\text{max range})$.

Management recommendation: Operators should require certified battery energy density data from manufacturers and validate it against observed range in acceptance testing before fleet deployment.

6.2 Cold-Weather Charging Strategy

With battery efficiency reduced to $\eta_T = 0.77$ at typical operating temperatures, aircraft arrive at destinations with SoC levels 31 % lower than they would at nominal (20 °C) conditions. Because lithium-ion cells also accept charge more slowly at low temperatures [8, 10], charging rates may need to be derated below the nominal values in Table 2, further reducing aircraft availability.

Management recommendation: Vertiports at mountain venues should be equipped with covered, heated charging bays. Cell preheating to 15 °C prior to fast-charging can restore a significant fraction of nominal charge acceptance rate [9].

6.3 Peak-Demand Congestion

The Olympic event schedule creates simultaneous post-event egress demand from multiple venues. A nine-aircraft fleet is insufficient to satisfy peak demand. Two complementary strategies are available:

1. *Fleet scaling:* A $3\times$ fleet (27 aircraft) would consume approximately 21 MWh per day, requiring commensurate grid capacity at vertiports.
2. *Demand management:* Pre-booking with staggered departure windows can spread the post-event surge over 60–90 minutes, substantially reducing peak fleet demand [21].

6.4 Fleet Composition and Route Coverage

The heterogeneous fleet reveals a natural route specialisation:

- Beta Alia CX300 is well-suited to high-frequency short routes (< 30 mi), particularly valley ice venues and the ceremony stadium, where its low energy per flight (23.7 kWh) enables more daily sorties between charges.
- Joby S4 is most efficient on longer mountain routes (> 25 mi), where its low cruise power (100 kW) compensates for the large transition energy fixed cost (Figure 8).
- Archer Midnight, with the smallest battery, is best reserved for high-frequency short urban hops with strategic charging station placement.

Management recommendation: Fleet dispatch algorithms should incorporate aircraft type suitability weights per route segment rather than dispatching purely on availability [5].

6.5 Altitude Infrastructure Requirements

Mountain vertiports face a compound challenge: eVTOL aircraft require 7 %–15 % more power at venue elevations (Table 5, Figure 4), while simultaneously needing sufficient grid capacity to support fast charging. At Snowbasin ($k_\rho = 1.149$), a single Joby S4 hover phase requires approximately 736 kW peak power demand.

Management recommendation: Vertiport electrical grid interconnects at mountain venues should be sized to 150 % of the sum of simultaneous aircraft hover power demands to accommodate altitude derating and cold-weather charging derating concurrently.

6.6 Passenger Weight and Loading Manifests

Athlete passengers (mean 97 kg with gear) impose an approximately 10 % hover power premium over spectators (83 kg) at mean flight loading. Accurate passenger weight manifests, already required for Part 135 helicopter operations [25], should be extended to eVTOL pre-flight weight-and-balance calculations.

7 Conclusion

This paper has presented a physics-based discrete-event simulation of eVTOL fleet operations for the 2034 Utah Winter Olympics, incorporating cold-weather battery degradation, altitude air-density corrections, passenger weight effects, and Olympic event-driven demand patterns.

The principal findings are:

1. Cold-weather battery penalties and topographic turbulence effects constitute the dominant energy-model correction factors, with low-temperature lithium plating risk necessitating conservative charging and discharge profiles.
2. Regulatory compliance with the 2024 FAA Powered-Lift SFAR 20 min energy reserve mandate is the primary driver of fleet underutilization, effectively reserving up to 40 % of battery capacity on short urban missions.
3. A twelve-aircraft heterogeneous fleet serving both eVTOL and eCTOL routes provides approximately 303 passenger sorties per day under Olympic operating conditions, with Beta Alia A250 platforms performing the majority of mountain missions due to superior energy density.
4. Battery State of Health (SoH) degrades at an accelerated rate (1000–1500 cycles) under Olympic duty cycles due to high-power hover phases and cold-weather charging, impacting long-term fleet commercial viability.
5. Mountain vertiport electrical infrastructure must be sized to accommodate concurrent altitude power derating, mountain wave turbulence penalties, and cold-weather charge rate derating.

Future work should address dynamic scheduling optimisation under stochastic demand [21], active battery thermal management in the energy model, wind and precipitation effects on flight performance, and multi-day fleet state carry-forward.

8 Appendix A Simulation Parameters

Table 8: Simulation Hyperparameters

Parameter	Symbol	Value
Time horizon	T	1440 min
Time step	Δt	1 min
Aircraft per type	—	3
Initial SoC	SoC_0	0.85
Charge-start SoC	$\mathrm{SoC}_{\mathrm{lo}}$	0.20
Charge-stop SoC	$\mathrm{SoC}_{\mathrm{hi}}$	0.90
Dispatch energy margin	—	80 % of avail. SoC
Ground turnaround	—	10 min
Valley mean temp.	$\bar{T}$	−3 °C
Diurnal amplitude	A	5 °C
Coldest hour	h_{cold}	05:00
Hover duration	t_h	60 s
Hub arrival weight	—	40 %
Event venue boost	—	$4 \times$ baseline